Available online at www.sciencedirect.com
SCIENCE DIRECT®
Journal of Sound and Vibration 269 (2004) 965–990
JOURNAL OF SOUND AND VIBRATION
www.elsevier.com/locate/jsvi

An analysis of interlaminar stresses in active constrained layer damping treatments

A. Badre-Alam[a], K.W. Wang[b,*], F. Gandhi[c]

[a] *Lord Corporation, Cary, NC, USA*
[b] *Department of Mechanical and Nuclear Engineering, The Pennsylvania State University, University Park, PA, USA*
[c] *Department of Aerospace Engineering, The Pennsylvania State University, University Park, PA, USA*

Received 26 December 2001; accepted 16 January 2003

Abstract

This paper presents an analysis of the interlaminar stresses in active constrained layer (ACL) damping treatments. The primary objective of this study is to provide in-depth understanding of the delamination of ACL damping treatment and, to establish guidelines to lower the risk of delamination without sacrificing performance. Two major issues are addressed in this investigation. First, the effects of feedback control schemes on interlaminar stresses are analyzed. The proportional (P) and the derivative (D) control laws are selected for comparison. It is found that for the system under consideration, for similar vibration reduction, the derivative control scheme introduces lower interlaminar stresses than proportional control. Also, the derivative control scheme has lower voltage requirements. Second, the ACL treatment is compared with the purely active configuration (without the viscoelastic layer). In addition to the damping performance and control effort requirement (which have been analyzed and compared by researchers in the past), the interlaminar stresses are now included in the comparison. It is shown that the ACL configuration could have significantly lower interlaminar stresses than the purely active configuration, for similar levels of vibration reduction. Hence, in applications where system durability is a concern, the ACL treatment should be preferred over purely active configuration because it has lower interlaminar stress as-well-as lower axial stresses in the piezoelectric cover sheet.

1. Background

The active constrained layer damping treatments have been investigated by many researchers as a means for structural vibration control and damping enhancement [1–12]. In such treatments, a

*Corresponding author. Structural Dynamics and Controls Laboratory, Pennsylvania State University, 137 Reber Building, University Park, PA, 16802-1412, USA. Fax: +1-814-863-7222.
E-mail address: kwwang@psu.edu (K.W. Wang).

0022-460X/03/$ - see front matter © 2003 Elsevier Ltd. All rights reserved.
doi:10.1016/S0022-460X(03)00208-6

viscoelastic material (VEM) layer is sandwiched between the host structure and a piezoelectric (in general, PZT is used) constraining layer. As the structure vibrates, a voltage input is applied to activate the PZT constraining layer based on feedback control, which induces axial strain in the PZT layer. This induced strain increases the shear deformation in the VEM layer and also exerts direct active forces on the structure. Both of these mechanisms (increased shear deformation and direct active forces) contribute to the vibration reduction. With proper phase adjustment, the emphasis on either one of these mechanisms can be increased.

Most of the efforts on ACL analysis have been focused on optimizing the vibration control performance of the treatment. It has been demonstrated that a judicious choice of VEM properties and geometric dimensions are necessary to guarantee superior performance (better than purely passive design and purely active configuration) [7–10]. It has also been shown that a careful attention to voltage limits is required in designing the system [11,12]. It is reasonable to believe that many of the parameters that affect the system damping performance can also affect the stresses in the treatment. If the stresses are too high, the treatment can break or delaminate. It has been documented that in purely active configurations (without the VEM), a slight debonding of the treatment can have a significant effect on the performance [13]. However, not much work has been done to address the stress distribution and reliability of ACL damping treatment. There are two obvious modes of failure for ACL. First, the PZT constraining layer can fail and break due to high axial stresses. This has been identified and considered previously [8,14]. Second, the ACL treatment can delaminate from the host structure due to high interlaminar stresses. This problem was identified by Lee and Lesieutre [15] but was not studied. In a paper published previously by the authors [16], the effect of some important design parameters on passive constrained layer (PCL) interlaminar stresses were analyzed and techniques were presented to reduce the stresses without sacrificing the damping performance. Despite its importance, the effect of active actions on the delamination behavior and interlaminar stresses of ACL damping treatments has yet to be investigated.

2. Objective

The objective of this research is to study the interlaminar stresses of ACL damping treatments under active controls. Specifically, this paper has two main focuses as stated below:

- Investigate the effect of control actions on the magnitude of the interlaminar stresses. To accomplish this task, the two common control schemes, proportional (P) and derivative (D), are analyzed and compared.
- Compare the interlaminar stresses in the ACL damping treatment with that in a purely active configuration (no VEM layer).

3. System description and mathematical model

This study is conducted on a fixed-free cantilever aluminum beam that is partly covered with ACL treatments on both sides (Fig. 1). The treatment covers 50% of the beam length as shown in

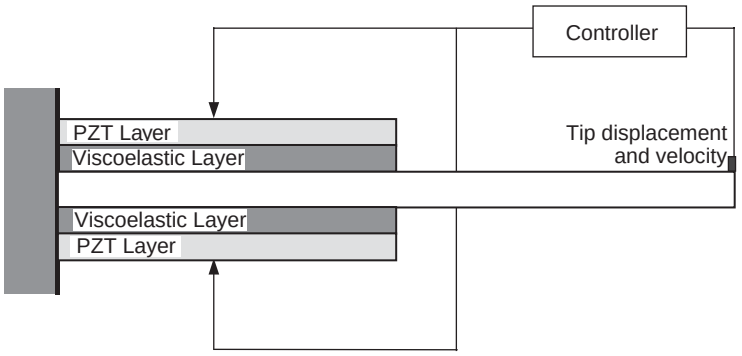

Fig. 1. Structure under consideration.

the figure. The constraining layer is made of PZT (American Piezo Ceramic—APC 850) and the shear layer is made of either 3MISD112 or DYAD-606 viscoelastic materials (VEM).

The mathematical model developed for this study is based on the built-up bar (BUB) theory [17,18]. In the BUB theory, each layer is modelled as an independent beam, and the interlaminar stress between two layers is defined as a product of the interlaminar stiffness (described later in this section) and the relative displacement between the layers at the interface. These interlaminar stiffness terms couple the independent beam equations to provide the coupled system equations. In order to use BUB theory for this study, the original model proposed by Mirman [17,18] had to be modified and advanced. There are three major improvements made in the original model. First, the current mathematical model is derived using the finite element method and hence the differential equations can be solved by considering only the geometric boundary conditions. This simplifies the solution process significantly since the original solution approach proposed by Mirman [19] required trial functions that satisfy all the boundary conditions. Such trial functions are not easy to develop due to complex nature of the interlaminar stresses. Second, while the original model [17,19] only considered static stresses, the present model includes inertial effects and hence has the capability to calculate the dynamic stresses and modal damping ratios. Third, in addition to elastic materials, viscoelastic (VEM) and piezoelectric (PZT) material layers are included in the present model (Mirman [17,18] only used elastic materials).

In this mathematical model, the base beam is made of elastic material and the constraining layer is made of PZT. The shear layer (VEM) is modelled using frequency-dependent complex shear modulus. The part of the beam that is covered with the treatment is modelled using a 5-layered element (discussed later) while the remaining part is modelled using beam-rod elements. The beam is discretized into 60 elements along the length. The length of the element progressively becomes smaller towards the free end of the treatment to capture high stress concentrations. In this study, the model is reduced using its first two modes and the static correction vector (discussed later).

3.1. Assumptions

The key assumptions of this mathematical model are: (1) all layers are modelled as separate beams having independent axial, transverse and shear deformations; (2) shear deformation in every layer is constant through the thickness; (3) the transverse strain (ε_{zz}) is zero in all layers; (4)

linear theory of elasticity, viscoelasticity and piezoelectricity are used; (5) the applied voltage is constant along the length of the PZT layer; (6) the material properties and thickness of the layers are constant along the beam; (7) the poling axis of the PZT is perpendicular to the beam axis; (8) the interlaminar peeling and sheering stress in the kth bond (between the layers k and $k+1$), when the adjacent layers are made of elastic or PZT materials, is defined as (the fundamental assumption of BUB theory):

$$\sigma_k^b = \mu_k(w_k - w_{k+1}), \quad \tau_k^b = \zeta_k(u_k^B - u_{k+1}^T). \tag{1}$$

Here, w and u represent the transverse and axial displacements. T and B represent the top and bottom surfaces of the layer. Superscript b identifies that the stress terms are for a bond layer. μ and ζ represent the normal and shear interlaminar stiffness parameters, respectively. The subscript k denotes the kth layer.

3.2. Kinematic relationship

The displacement field in the kth layer of the structure can be expressed as

$$u_k = u_k^0 - z\left(\frac{\partial w_k^0}{\partial x} - \beta_k\right), \quad w_k = w_k^0, \tag{2}$$

where u is the axial displacement, w is the transverse displacement and β is the shear angle. The subscript k denotes the kth layer and superscript o denotes the neutral axis of the kth layer. z is the distance from the neutral axis of the kth layer (which is midway though the thickness).

3.3. Strain–displacement relationship

The strain-displacement relationship for the kth layer can be obtained by taking derivatives of Eq. (2). Thus

$$\varepsilon_k = \frac{\partial u_k}{\partial x} = \frac{\partial u_k^0}{\partial x} - z\left(\frac{\partial^2 w_k^0}{\partial x^2} - \frac{\partial \beta_k}{\partial x}\right),$$

$$\gamma_k = \frac{\partial u_k}{\partial z} + \frac{\partial w_k^0}{\partial x} = -\beta_k, \tag{3a, b}$$

where ε and γ are the normal and shear strains in the laminate.

3.4. Stress–strain relationships

The stress–strain relationship in a layer is dependent on the type of the material that particular layer is made of. The stress strain relations for the layers made with elastic material is represented by Hooke's Law,

$$\begin{Bmatrix} \sigma_k \\ \tau_k \end{Bmatrix} = \begin{bmatrix} E_k & 0 \\ 0 & G_k \end{bmatrix} \begin{Bmatrix} \varepsilon_k \\ \gamma_k \end{Bmatrix}, \tag{4}$$

where E and G are the Young's modulus and the shear modulus of elasticity, respectively. σ_k and τ_k are the axial and the shear stress in the kth layer.

The stress and strain in a viscoelastic layer are related to each other by

$$\begin{Bmatrix} \sigma_k^* \\ \tau_k^* \end{Bmatrix} = \begin{bmatrix} E_k^* & 0 \\ 0 & G_k^* \end{bmatrix} \begin{Bmatrix} \varepsilon_k \\ \gamma_k \end{Bmatrix}, \tag{5}$$

where E^* and G^* are the complex normal and shear elastic modulus. Since, these two parameters are frequency-dependent, their value at a certain frequency is obtained from a look-up table that is developed using the manufacturers data for 3MISD112 and DYAD-606.

The stress and strain in a PZT material are related by the constitutive equation of the piezoelectric materials [IEEE Standard on Piezoelectricity, 1987]:

$$\begin{Bmatrix} \sigma_k \\ \tau_k \\ E_k \end{Bmatrix} = \begin{bmatrix} C_{11}^D & 0 & -h_{31} \\ 0 & C_{55}^D & 0 \\ -h_{31} & 0 & \beta_{33}^s \end{bmatrix} \begin{Bmatrix} \varepsilon_k \\ \gamma_k \\ D_k \end{Bmatrix}. \tag{6}$$

Here, E_k represents the electrical field across the kth layer. D_k represents the electrical charge on the kth layer. C_{11}^D represents the open circuit axial elastic modulus. C_{55}^D represents the open circuit shear modulus. β_{33}^s is the dielectric constant and h_{31} is the piezoelectric constant.

3.5. Potential energy

The potential energy of a layer is dependent on the material of that layer. The potential energy of the kth layer made of an elastic material is

$$U_k = \frac{1}{2}\int_0^{Le} \left[E_k A_k \left(\frac{\partial u_k^0}{\partial x}\right)^2 + E_k I_k \left(\frac{\partial^2 w_k}{\partial x^2} - \frac{\partial \beta_k}{\partial x}\right)^2 + G_k A_k (\beta_k)^2 \right] \mathrm{d}x. \tag{7}$$

The potential energy of the kth layer made of a PZT material is:

$$\begin{aligned} U_k = \frac{1}{2}\int_0^{Le} \Bigg[& C_{11}^D A_k \left(\frac{\partial u_k^0}{\partial x}\right)^2 + C_{11}^D I_k \left(\frac{\partial^2 w_k}{\partial x^2} - \frac{\partial \beta_k}{\partial x}\right)^2 + C_{55}^D A_k (\beta_k)^2 \\ & - 2A_k h_{31} D_k \left(\frac{\partial u_k}{\partial x}\right) + A_k \beta_{33} (D_k)^2 \Bigg] \mathrm{d}x \end{aligned} \tag{8}$$

Here, Le is the length of the element. A_k *and* I_k are the area and moment of inertia (around the neutral axis of the layer) respectively. The elastic and dissipative energy associated with the VEM layers is included in the virtual work term.

3.6. Kinetic energy

The kinetic energy expression is similar for all the layers. It is only dependent on the density ρ and the kinematic degrees of freedom. It can be represented as

$$T_k = \frac{1}{2}\int_0^{Le} \rho_k \left[A_k \left(\frac{\partial u_k}{\partial t}\right)^2 + I_k \left(\frac{\partial^2 w_k}{\partial x \partial t} - \frac{\partial \beta_k}{\partial t}\right)^2 + A_k \left(\frac{\partial w_k}{\partial t}\right)^2 \right] \mathrm{d}x. \tag{9}$$

3.7. Virtual work

The virtual work done on the kth layer made of a viscoelastic material is

$$\delta W_k = \frac{1}{2}\int_0^{Le}\left[E_k^* A_k\left(\frac{\partial u_k^0}{\partial x}\right)\delta\left(\frac{\partial u_k^0}{\partial x}\right) + E_k^* I_k\left(\frac{\partial^2 w_k}{\partial x^2} - \frac{\partial \beta_k}{\partial x}\right)\delta\left(\frac{\partial^2 w_k}{\partial x^2} - \frac{\partial \beta_k}{\partial x}\right) + G_k^* A_k(\beta_k)\delta(\beta_k)\right] \mathrm{d}x. \tag{10}$$

The virtual work done on a bond between two layers, $(k-1)$th and kth, due to the interlaminar stiffness is represented by

$$\delta W_{k-1}^J = \int_0^{Le} b\left[\mu_{k-1}(w_{k-1} - w_k)\delta(w_{k-1} - w_k) + \zeta_{k-1}(u_{k-1}^B - u_k^T)\delta(u_{k-1}^B - u_k^T)\right] \mathrm{d}x, \tag{11}$$

where the superscripts, T and B, represent the top and bottom of the layer, respectively. b in the above equation is the width of the layer. The bond between the $(k-1)$th and kth layers is denoted as bond $k-1$ (e.g., bond 1 is between the first and the second layers).

If the kth layer is made of PZT, the virtual work done on the layer by the applied voltage can be represented by

$$\delta W_k = \int_0^{Le} b V_k \delta D_k \, \mathrm{d}x. \tag{12}$$

3.8. Concept of interlaminar stiffness

The interlaminar stiffness μ and ζ used in the virtual work expression (Eq. (11)) were first introduced by Suhir [19,20]. In those studies, he presented an analytical derivation to determine the value of interlaminar stiffness parameters for thin laminates. Pao and Esele [21] presented the modifications for these parameters when multiple layers were used. Lee and Mirman [22] discussed the theory in more detail and showed that, while the actual parameters do require some experimental measurements, the approximations used by other researchers (including Suhir [20]) were sufficiently accurate for most analyses.

In the BUB theory, it is assumed that each layer behaves like an independent beam and is connected to adjacent layers by a distributed spring. The spring connection between the layers accounts for the transverse and shear compliance between the neutral axes of two adjacent layers. The spring constant is calculated using the spring-in-series concept. For the bond $k-1$, which is between the elastic layers $k-1$ and k, the interlaminar stiffness parameters are:

$$\mu_k = \left(\frac{\delta_a h_a}{E_a} + \frac{1}{\kappa}\left(\frac{\delta_{k-1} h_{k-1}}{E_{k-1}} + \frac{\delta_k h_k}{E_k}\right)\right)^{-1}, \tag{13a}$$

$$\zeta_k = \left(\frac{\alpha_a h_a}{G_a} + \frac{1}{\kappa}\left(\frac{\alpha_{k-1} h_{k-1}}{G_{k-1}} + \frac{\alpha_k h_k}{G_k}\right)\right)^{-1}, \tag{13b}$$

where h is the thickness of the particular layer, E and G are the modulus of elasticity and shear modulus, respectively. δ and α are correction parameters. Pao and Esele [21] used this parameter (δ) to correct the value of the interlaminar stiffness depending on the layer location within the laminate: $\delta = 2$ for the top and bottom layers and $\delta = 1$ for the intermediate layers. Since the outer layers only have one surface bonded, the interlaminar stiffness is half as compared to the layers that have both surfaces bonded within the laminate. κ is a multiplication factor and was given a value of 3 in Suhir's analysis [20]. Lee and Mirman [22] discussed the significance of the multiplication factor and mentioned that various researchers have used different values for this parameter. In the present study, the value of 3 previously used by Suhir [20] and later by Pao and Eisele [21] is used. The subscript a denotes the adhesive layer. It can be seen from the above equation that if the adhesive is very thin and stiff as compared to the VEM, its contribution to the interlaminar stiffness is negligible (an assumption in this study).

3.9. Interlaminar stiffness involving VEM layers

The interlaminar stiffness parameters discussed above can also be used when one of the layer is made of VEM. In such a case, the frequency-dependent complex modulus of VEM can be used in Eq. (13). This will provide complex frequency-dependent interlaminar stiffness parameters that can be used in Eq. (11).

3.10. Finite element equations

In order to develop the finite element equations of motion, the potential energy, kinetic energy and virtual work expressions for all the layers and the interlaminar bonds are used in the Hamilton's principle formulation. The dynamic variables in energy and work expressions, structural displacements and electrical charge, are approximated using nodal parameters and shape functions. The shape functions represent the variation of parameters within each element. In this model, the transverse displacement is approximated using a cubic shape function; the axial displacement, shear angle and the electric charge are approximated using a quadratic shape functions. This choice of shape functions provides convergence of the solution with a reasonable number of elements. Once assembled, the global finite element equations can be expressed as

$$[M]\{\ddot{\bar{q}}\} + [K^*(\omega)]\{\bar{q}\} = \{F\} + \{E\}V_p, \tag{14}$$

where $\{\bar{q}\}$and $\{\ddot{\bar{q}}\}$ are nodal displacement and acceleration vectors respectively. V_p is the voltage across PZT. The vector $\{F\}$ is the external force vector. $[M]$ is the mass matrix and $[K^*]$ is complex stiffness matrix.

3.11. Modal reduction

The interlaminar stresses in the structure are concentrated in small regions close to the free end. To accurately capture these stresses, the finite element discretization has to be highly refined (small element size) in close vicinity of these stress concentrations. Thus, the finite element model developed to calculate the interlaminar stresses usually tends to have very large dimensions. In this analysis, the dimensions of the finite element model are reduced to decrease the computational effort required for the parametric study of the control system.

For the present system, classical modal reduction methods cannot be applied directly due to three main issues. First, in this model, the VEM has frequency-dependent material properties and thus simple eigenvalues and eigenvectors cannot be calculated using traditional methods. Second, even without frequency-dependent material properties, a classical reduced order model cannot capture the localized deformations and stresses with only the first few modes. Third, if active control laws were implemented on the reduced order model with only a few modes, the errors in the solution could be significant [23]. On the other hand, if a large number of structural modes were used, the computational effort would again be very high. To address these issues, several techniques are utilized, as described in the following paragraphs.

First, the iterative procedure presented by Friswell and Inman [24] is used to derive the eigenvectors. In this technique, the eigenvectors and modal parameters of each mode are calculated using the VEM stiffness at the natural frequency of that mode. Since the natural frequency of the mode is not initially known, the system stiffness matrix cannot be calculated. Thus, the eigenvectors and modal parameters of the system are obtained in a recursive manner. An initial estimate of the eigenvalue is made using the static stiffness properties of the VEM. Then new VEM stiffness parameters are calculated at the natural frequency obtained from the initial estimate of the eigenvalue. These new VEM stiffness properties are then used to develop an updated system stiffness matrix. Eigenvalues and modal vectors are calculated again and, the new eigenvalues are compared with the previous ones. This process is continued until convergence is achieved (0.1% difference in the amplitude of eigenvalue). Once the eigenvalue is converged, the modal parameters for that mode are calculated using the mode shape and system matrices. The ith modal equation will be

$$m_i\ddot{p}_i + k_i^* p_i = f_i + e_i V_p, \tag{15}$$

where m, k^*, f and e are the modal mass, complex modal stiffness and modal forcing and control functions, respectively.

It is documented by Ponslet et al. [23] and Plouin and Balmes [25] that to correctly predict the localized deformation due to active control actions, a large number of normal modes are required. However, if a static correction vector (Ritz vector) is used together with the normal modes in the projection matrix, accurate results of the structural deformation can be obtained by using only a few modes. Hence, in this study, the system is reduced using a Ritz vector and two modal vectors. Since the stiffness matrix is frequency dependent, the Ritz vector is calculated using the system stiffness evaluated at the first natural frequency (the main frequency of interest).

$$b = \left[K^*(\omega_1)\right]^{-1}\{E\}, \tag{16}$$

where b is the Ritz vector, K^* is complex stiffness matrix, ω_1 is the first natural frequency and E is the unit control force.

To avoid including the contribution of the first mode again, the orthogonal component of this vector to the first eigenvector is calculated.

$$b_0 = b - b\phi_1, \tag{17}$$

where, ϕ_1 is the unit vector in the direction of the first eigenvector. This modified Ritz vector is used in the model reduction in a similar manner that an eigenvector would be used.

$$b_o^T[M]b_o\ddot{p}_b + b_o^T[K(\omega_1)]b_o p_b = b_o^T\{F\} + b_o^T\{E\}V_p. \tag{18}$$

The complete reduced order model is

$$\begin{bmatrix} m_1 & 0 & 0 \\ 0 & m_2 & 0 \\ 0 & 0 & m_b \end{bmatrix} \begin{Bmatrix} \ddot{p}_1 \\ \ddot{p}_2 \\ \ddot{p}_b \end{Bmatrix} + \begin{bmatrix} k_1^* & 0 & 0 \\ 0 & k_2^* & 0 \\ 0 & 0 & k_b^* \end{bmatrix} \begin{Bmatrix} p_1 \\ p_2 \\ p_b \end{Bmatrix} = \begin{Bmatrix} f_1 \\ f_2 \\ f_b \end{Bmatrix} + \begin{Bmatrix} e_1 \\ e_2 \\ e_b \end{Bmatrix} V_p, \tag{19}$$

where the subscripts 1,2 and b are used to represent the first and second eigensolutions and the static correction of the system, respectively. It is verified that this reduced order model has a good correlation with the full size model for both passive damping (constrained layer treatment without active control input) and closed-loop control scenarios [26].

4. System analysis

The system parameters used in this analysis are illustrated in Table 1. The 3MISD112 VEM is used in most of the investigations (Figs. 2–13 and 20–23) while DYAD-606 is used as VEM in the other case studies (Figs. 14–19). The interlaminar stiffness parameters at the first natural frequency are listed in Table 2 for the top two interfaces. The value of these parameters for the bottom two interfaces is the same as those of the top two due to system symmetry. Since the values of these parameters are dependent on the modulus of VEM layer, which are frequency dependent, their value is not constant. For the purpose of analysis, the VEM thickness is selected to be optimum for passive damping (best fail safe property with no active action). Fig. 2 shows the system passive damping (1st mode critical damping ratio) as a function of the 3MISD112 VEM thickness. It can be seen in this figure that the optimum value of VEM thickness is 0.149 mm and the maximum damping for this thickness is 10.76% (Figs. 2–23).

Table 1
System parameters

C_{11}^D	76.16 GPa
C_{11}^E	65.36 GPa
d_{31}	−1.75 e−10
E_b	70 Gpa
E_v	3MISD112 or DYAD-606
E_a	2.33 GPa
t_c	0.764 mm
t_v	0.149 mm
t_b	3.0734 mm
L	7 in
ρ_b	2710 kg/m^3
ρ_v	1250 kg/m^3
ρ_c	7500 kg/m^3
v_c	0
v_b	0
v_v	0.5

Table 2
Interlaminar stiffness at ω_1

β_1	$3.62 \times 10^9 + \mathrm{i}3.69 \times 10^9$ Pa
β_2	$3.62 \times 10^9 + \mathrm{i}3.69 \times 10^9$ Pa
γ_1	$4.83 \times 10^9 + \mathrm{i}4.92 \times 10^9$ Pa
γ_2	$4.83 \times 10^9 + \mathrm{i}4.92 \times 10^9$ Pa

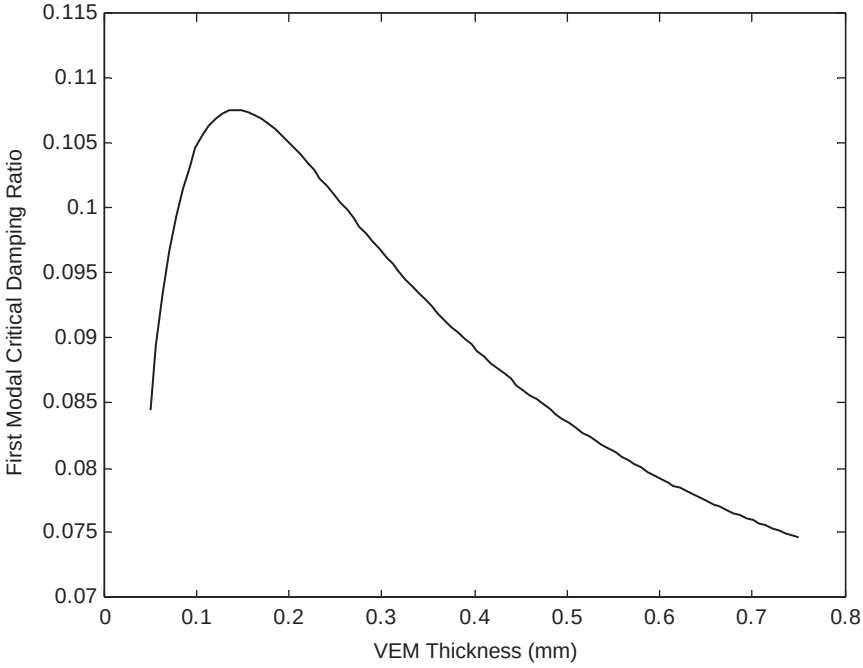

Fig. 2. Passive damping as a function of viscoelastic material layer thickness. Optimum $t_v = 0.149$ mm and $\xi = 10.76\%$.

Exciting the beam at its first resonance with unit harmonic tip force, the amplitudes of the interlaminar peeling stresses between the PZT constraining layer and the VEM (PZT–VEM) and between the VEM and the beam (VEM–beam), are shown in Fig. 3. It can be seen that there is a high peeling stress concentration close to the free end of the treatment. This high stress region, also know as a region of stress singularity, is common for structures with bonded joints and laminates [17–19]. The phase of the response due to damping is not shown in this paper. The interlaminar shearing stress for similar loading condition is shown in Fig. 4. This figure illustrates that the interlaminar shearing stress does not have a distinct region of high stress concentration and, the stress is more evenly distributed along the length of the beam (nearly linear and without singularity). Also, the interlaminar shearing stress values are the same for all the interfaces. This characteristic of the interlaminar shearing stress is due to the low shear stiffness of the VEM layer.

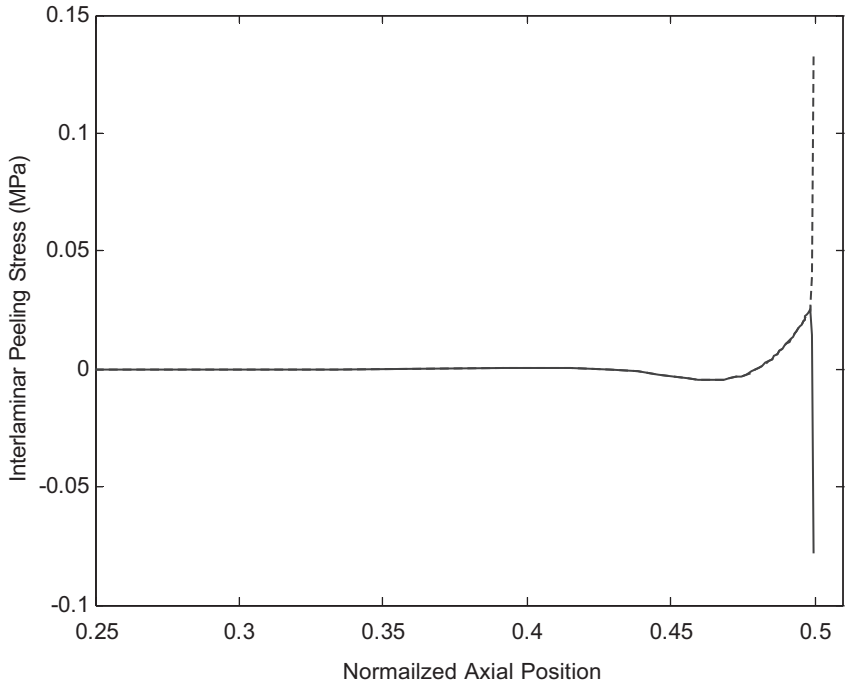

Fig. 3. Interlaminar peeling stress for a unit tip transverse force—passive damping case with constrained layer treatment but no active control input. VEM–beam (– – –), PZT-VEM (——).

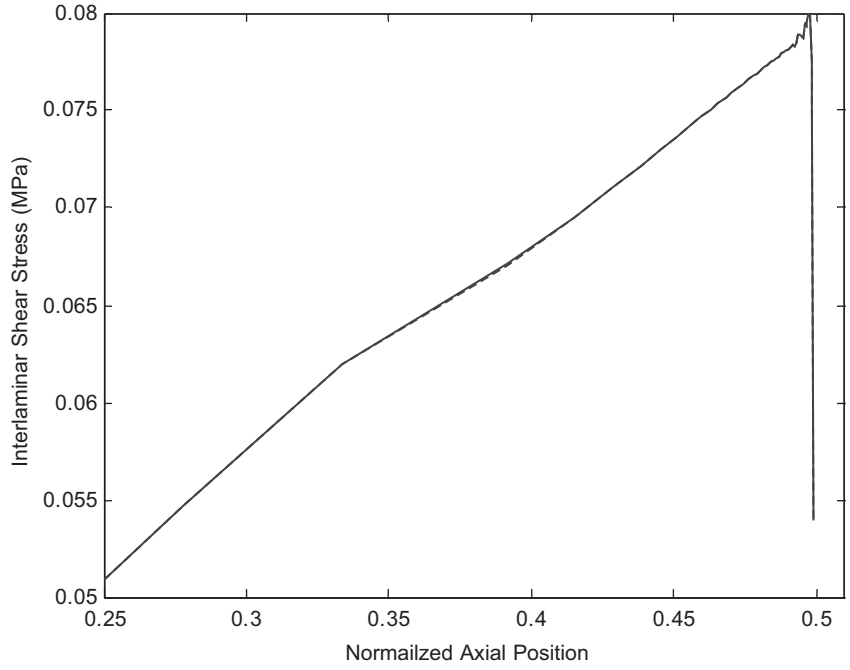

Fig. 4. Interlaminar shearing stress for a unit tip transverse force—passive damping case with constrained layer treatment but no active control input. VEM–beam (– – – –), PZT–VEM (——), the two curves are coincident.

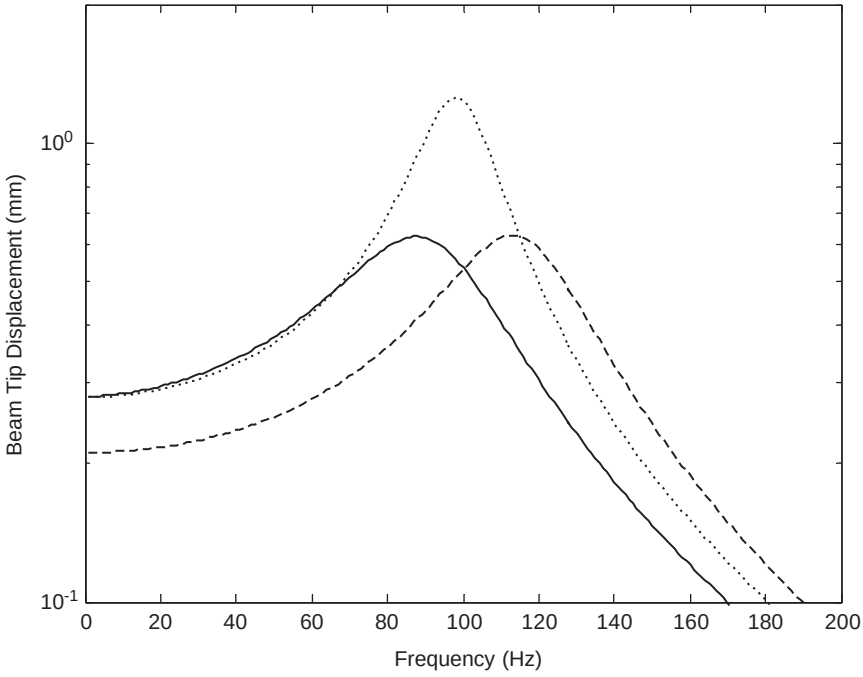

Fig. 5. Frequency response function of beam tip displacement for unit tip load. Passive damping ($\cdots$) resonant-amplitude = 1.3 mm and $\xi = 10.76\%$; *D*-control (——) resonant-amplitude = 0.63 mm, $\xi = 23.03\%$ and $Kd = 809$; *P*-control (– – – –) resonant-amplitude = 0.63 mm, $\xi = 16.12\%$ and $Kp = 6.65 \times 10^5$.

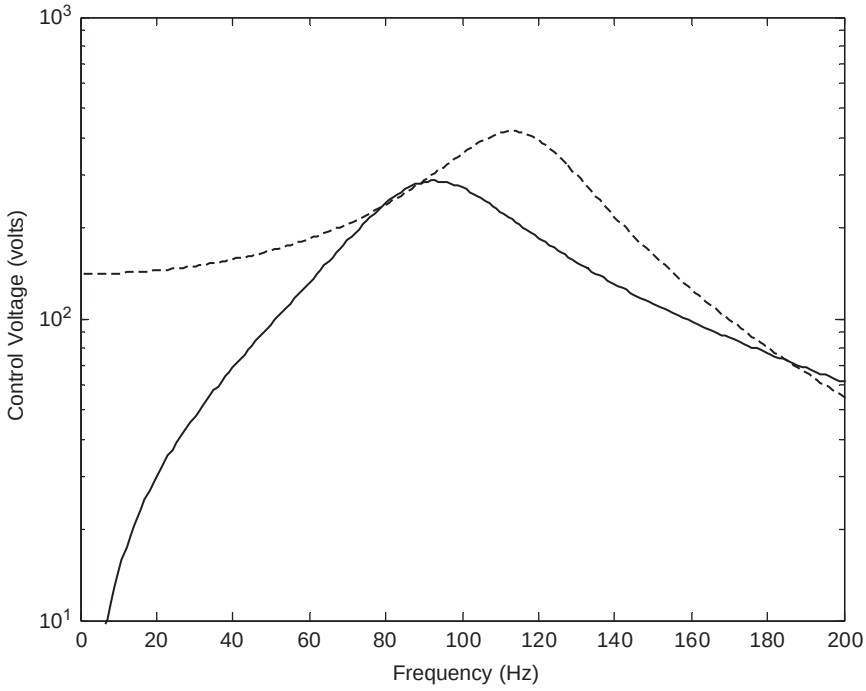

Fig. 6. Frequency response function of control voltage for unit tip load. *D*-control (——) resonant-amplitude = 286 V for $Kd = 809$; *P*-control (– – – –) resonant-amplitude = 418 V for $Kp = 6.65 \times 10^5$.

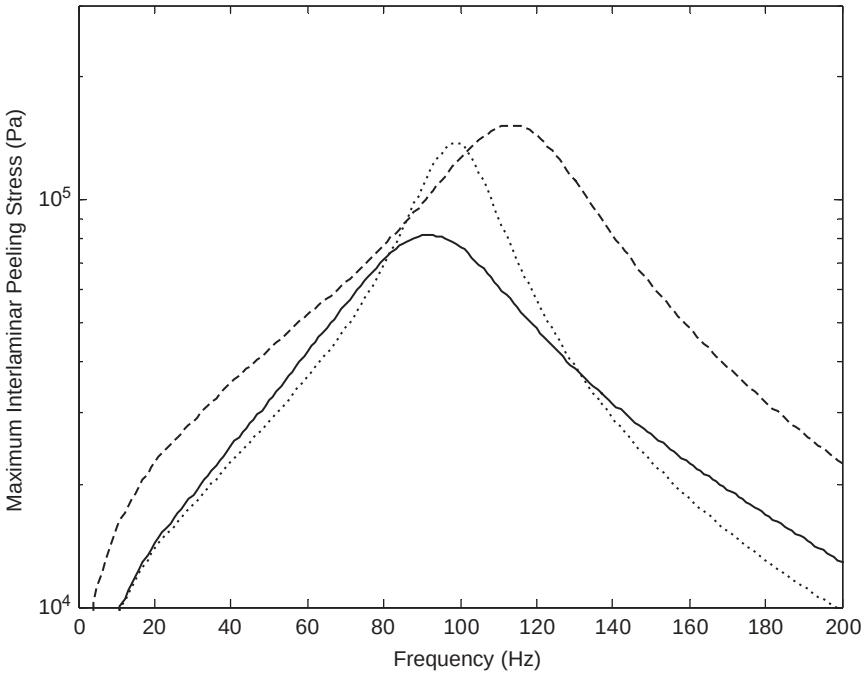

Fig. 7. Amplitude of interlaminar peeling stress between constraining and VEM layers for unit tip load. Passive damping ($\cdots$) resonant-amplitude $= 1.38 \times 10^5$ Pa; D-control (——) resonant-amplitude $= 8.2 \times 10^4$ Pa for $Kd = 809$; P-control (– – – –) resonant-amplitude $= 1.53 \times 10^5$ Pa for $Kp = 6.65 \times 10^5$.

4.1. Comparison between P and D controls

In order to analyze the effect of active action on the durability of the ACL treatment, the amplitudes of interlaminar stresses (both peeling and shearing) are studied in an actively controlled system. Two control schemes, the derivative (D) and the proportional (P), are selected for this study, since they augment the baseline passive damping by different mechanisms. Philosophically stating, P control is aiming at increasing the shear angle in the VEM layer, while D control is synthesized to generate direct dissipative active forces. Due to this difference, their effects on the interlaminar stresses are different. The stresses and performance of these two control schemes are compared with each other and to the baseline passive damping case. Throughout this paper, the baseline passive damping configuration is defined to be the system with constrained layer damping treatment (PZT coversheet and VEM layer) but without active control inputs. Since the objective of a closed loop control is to reduce structural vibration, it is important to analyze the magnitude of interlaminar stress in relation to the vibration reduction performance. Thus, performance parameters, in terms of vibration reduction have to be established. In this study, the primary parameter selected for evaluation is the reduction in the beam tip displacement in comparison to the passive damping configuration, under a unit tip transverse force. Since the beam tip displacement can be calculated for frequencies around the first natural frequency, the largest displacement in this near resonance range is used. In this paper, it is referred to as the "maximum" tip transverse displacement. Similarly, "maximum" stress and

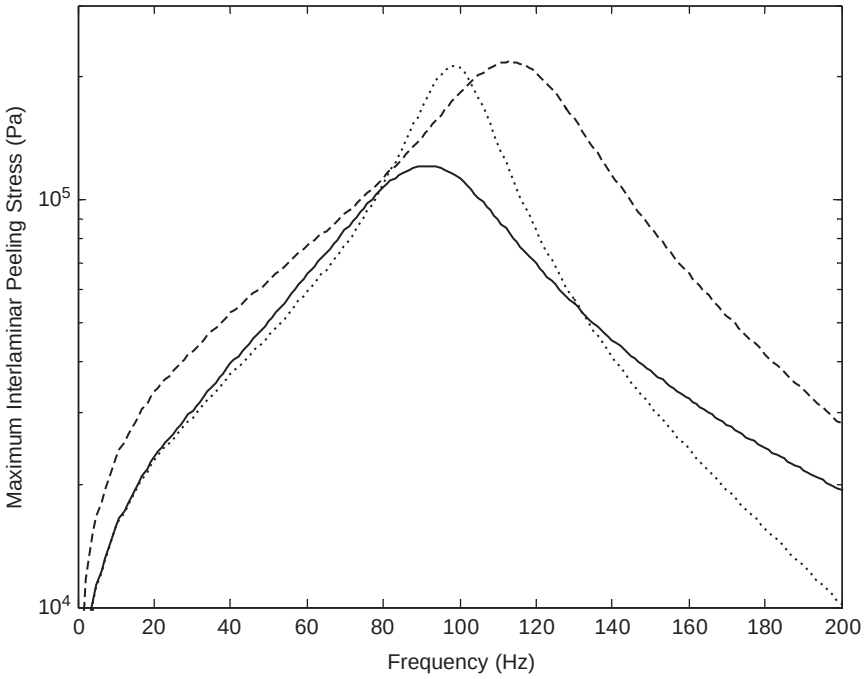

Fig. 8. Amplitude of peeling stress between VEM layer and beam for unit tip load. Passive damping (· · · ·) resonant-amplitude = 2.13×10^5 Pa; *D*-control (——) resonant-amplitude = 8.2×10^4 Pa for $Kd = 809$; *P*-Control (– – – –) resonant-amplitude = 2.18×10^5 Pa for $Kp = 6.65 \times 10^5$.

voltage are defined as the maximum stress and voltage values in their frequency spectrums around the first resonance, respectively. Fig. 5 shows the frequency response of the beam tip displacement under a unit tip transverse force. It is plotted for the passive damping case, and for the derivative control and proportional control cases. The control gains are selected such that the reduction in the maximum tip transverse displacement, as compared to the passive damping case, is the same for both derivative and proportional control schemes (for this example, the reduction is 51.5%). It can be seen that both derivative and proportional controls provides significant vibration reduction. Fig. 6 shows the voltage requirements for these two cases under consideration. It can be seen that the maximum voltage requirements for derivative control is 31.5% lower than that of the proportional control. Figs. 7 and 8 show the peak interlaminar peeling stress for these two configurations at the two interfaces, PZT–VEM and VEM–beam, respectively. It can be seen in these figures that the maximum peeling stress for derivative control is 46.5% and 62.5% lower than that for proportional control for the respective interfaces. Also, when compared to the passive damping configuration, it can be seen that the derivative control reduces the maximum interlaminar peeling stress (by 40% and 61.5%) while the proportional control results in a small increase in interlaminar stresses. The reduction in interlaminar stresses with derivative control is due to the reduction of the structural resonant response of the closed-loop system in comparison to the passive damping system. For proportional control, there are two dominant factors that contribute to the peak interlaminar peeling stress. First, lowering the resonant response reduces the interlaminar stresses. Second, the active action directly increases the shear deformation in the

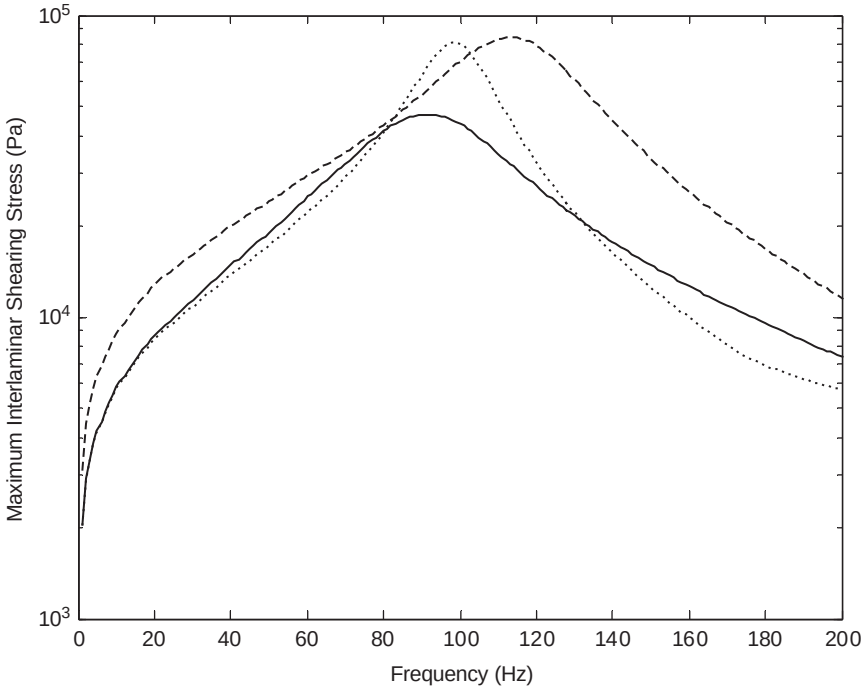

Fig. 9. Amplitude of shearing stress at both interfaces, PZT–VEM and VEM–beam, for unit tip load. Passive damping (· · · ·) resonant-amplitude = 8.07×10^4 Pa; *D*-control (——) resonant-amplitude = 4.69×10^4 Pa for $Kd = 809$; *P*-control (– – – –) resonant-amplitude = 8.44×10^4 Pa for $Kp = 6.65 \times 10^5$.

VEM [11,12] and thus increases the interlaminar stresses [26]. In the *P*-control scheme, the later factor is more dominant and thus the combined effect will cause a net increase in the interlaminar stresses, while the *D*-control hardly increase the shear at all [11,12].

The interlaminar shearing stress is the same for the two interfaces (PZT–VEM and VEM–beam). The peak value of the interlaminar shearing stress as a function of frequency is shown in Fig. 9. It can be seen in this figure that the maximum interlaminar shearing stress for derivative control is 44.5% lower than that for proportional control.

The analysis of the ACL treatment shown above demonstrates that the derivative control scheme has lower voltage requirement as well as lower interlaminar stresses (both peeling and shearing) for the cases under consideration. This is an important observation and it needs to be ascertained that it holds true for the other cases with different values of reduction in maximum beam tip displacements. The control voltage and the interlaminar stresses are next analyzed for a reasonable range of beam tip vibration reduction (0–5 dB, where 3 dB corresponds to 50%). To calculate the decibel value, the reference is chosen to be the maximum beam tip displacement of the passive damping system (1.3 mm), which is significantly lower than that of a system without any damping treatment. Fig. 10 shows the maximum voltage requirement as a function of beam tip displacement reduction for the two control schemes (the control voltage for tip displacement reduction of 3.14 dB corresponds to the maximum value in Fig. 6). It can be seen in Fig. 10 that the voltage requirement of derivative control is less than that of proportional control for this

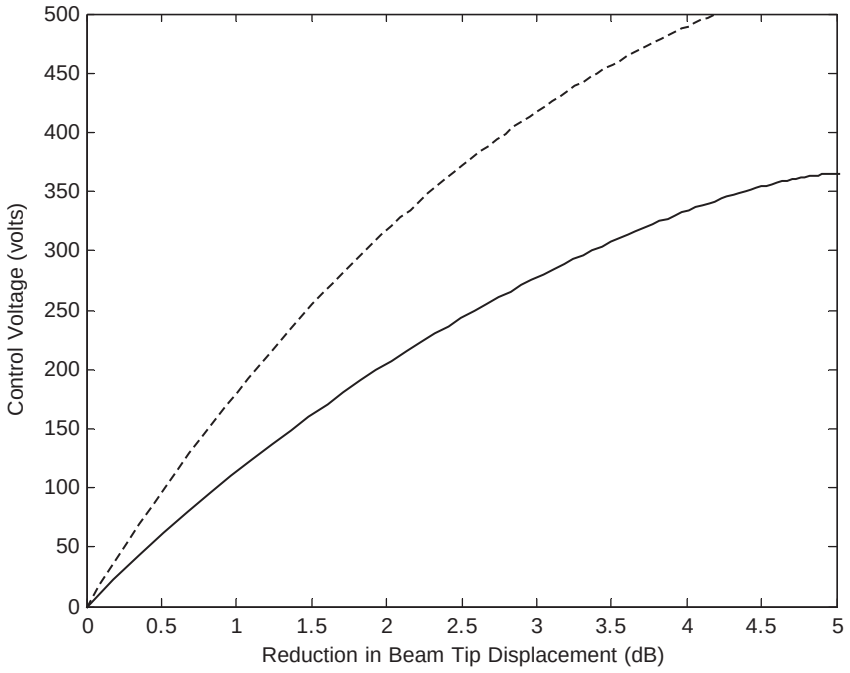

Fig. 10. Voltage requirements for derivative (——) and proportional (– – – –) control schemes.

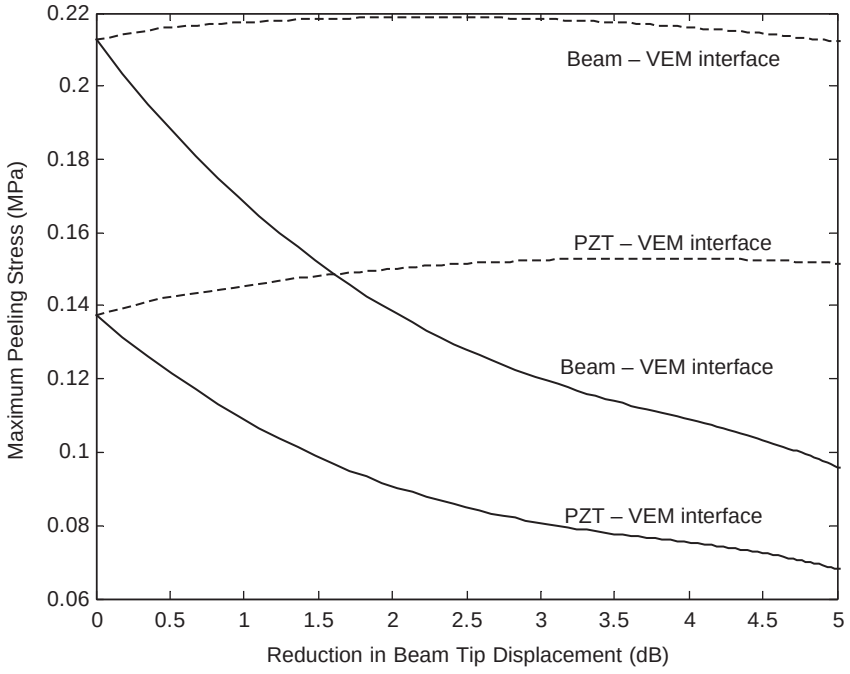

Fig. 11. Interlaminar peeling stress for derivative (——) and proportional (– – – –) control schemes.

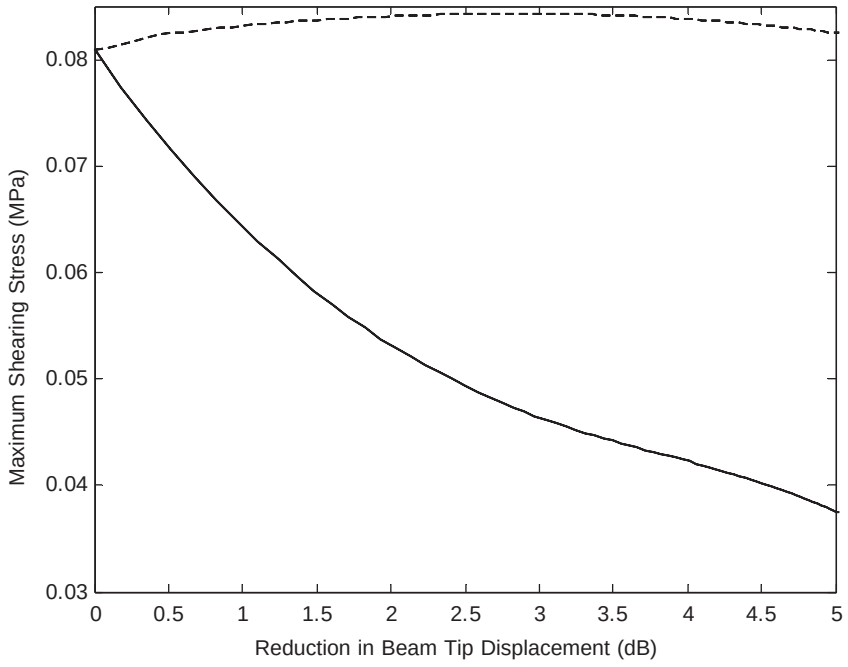

Fig. 12. Interlaminar shearing stress for derivative (——) and proportional (– – – –) control schemes.

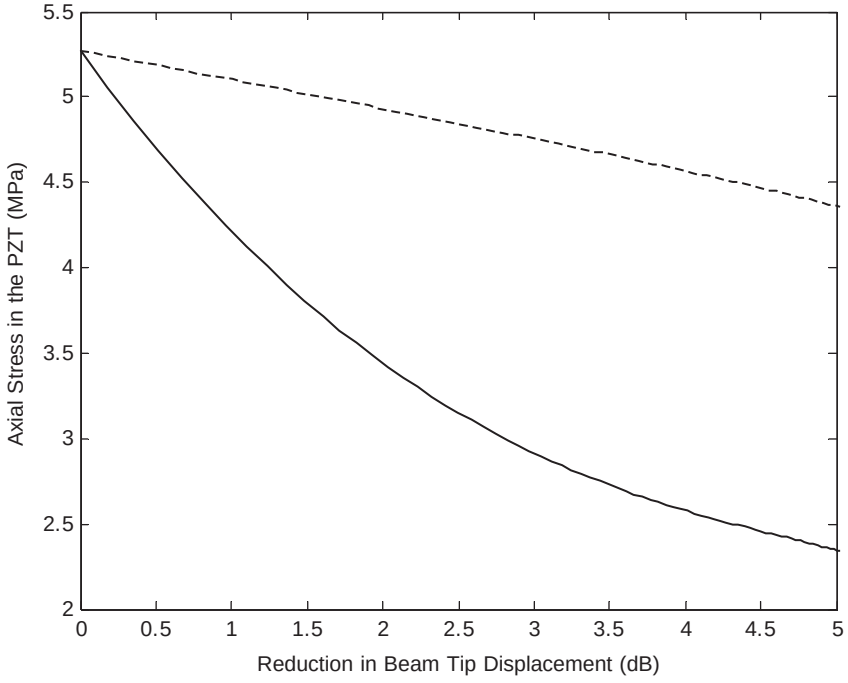

Fig. 13. PZT actuator axial stress for derivative (——) and proportional (– – – –) control schemes.

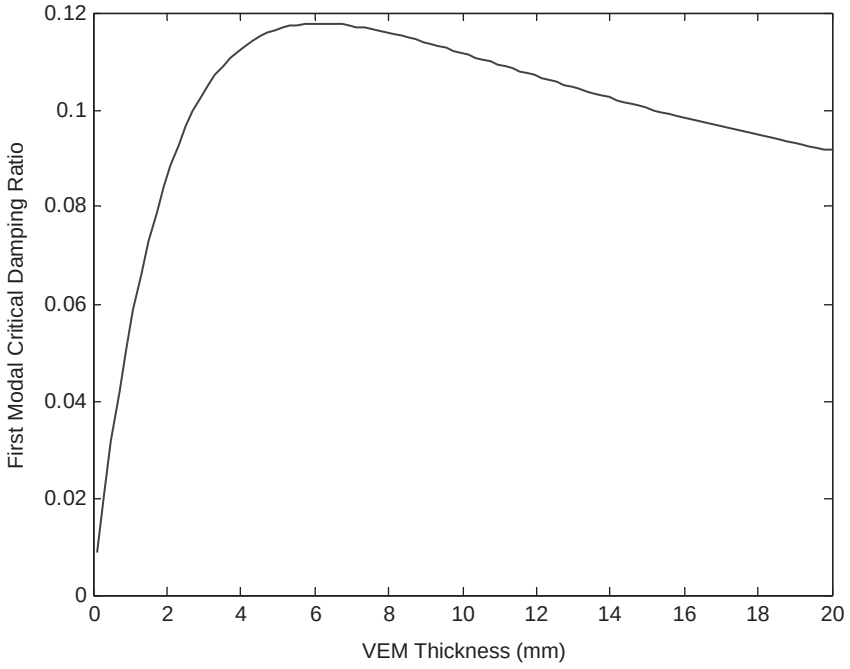

Fig. 14. Passive damping as a function of viscoelastic material layer thickness. Optimum $t_v = 5.9\,\text{mm}$ and $\xi = 11.78\%$.

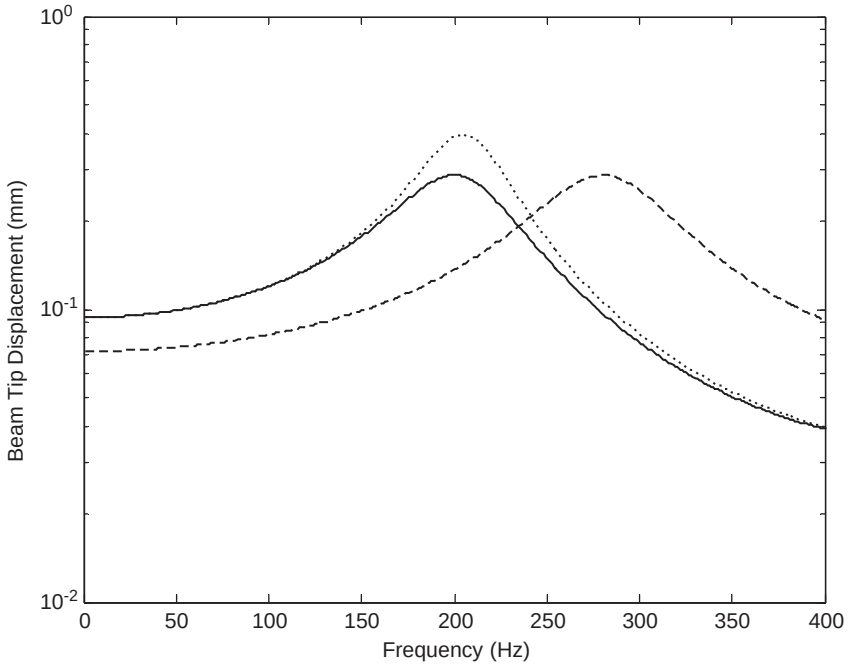

Fig. 15. Frequency response function of beam tip displacement for unit tip load. Passive damping (· · · ·) resonant-amplitude = 0.395 mm and $\xi = 11.78\%$; *D*-control (——) resonant-amplitude = 0.287 mm, $\xi = 16.38\%$ and $Kd = 191$; *P*-control (– – – –) resonant-amplitude = 0.287 mm, $\xi = 13.52\%$ and $Kp = 1.5 \times 10^4$.

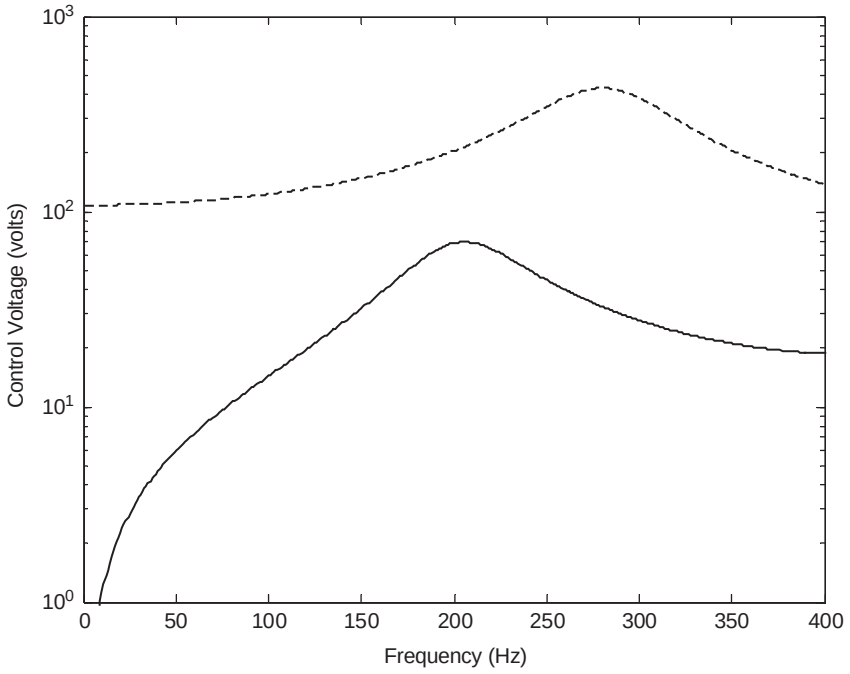

Fig. 16. Frequency response function of control voltage for tip transverse load. *D*-control (——) resonant-amplitude = 69.66 V for $Kd = 191$; *P*-control (- - - -) resonant-amplitude = 430.13 V for $Kp = 1.5 \times 10^6$.

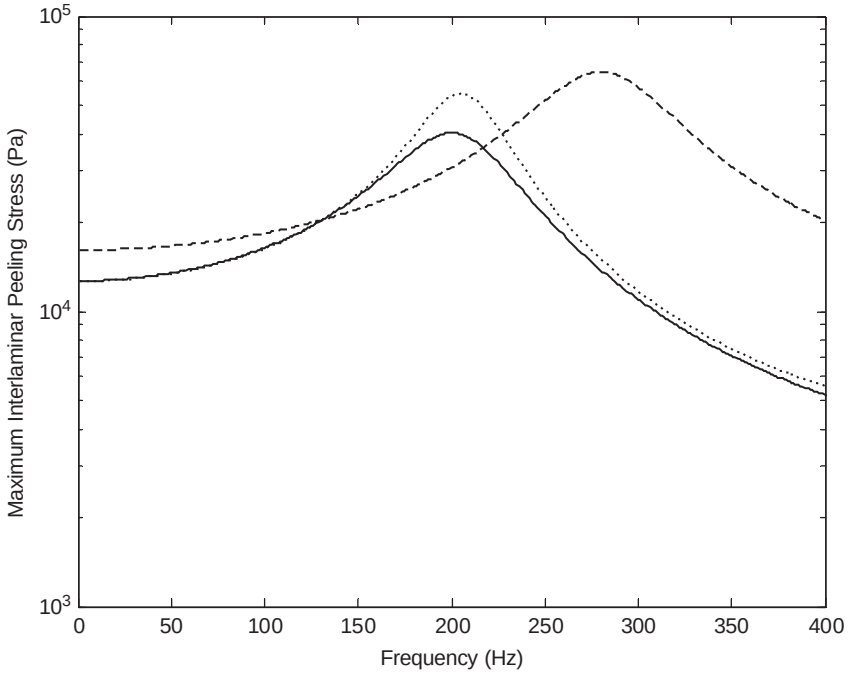

Fig. 17. Amplitude of peeling stress between constraining and VEM layers for unit tip transverse load. Passive damping (· · · ·) resonant-amplitude = 5.46×10^4 Pa; *D*-control (——) resonant-amplitude = 4.027×10^4 Pa for $Kd = 191$; *P*-control (– – – –) max amplitude = 6.47×10^4 Pa for $Kp = 1.5 \times 10^6$.

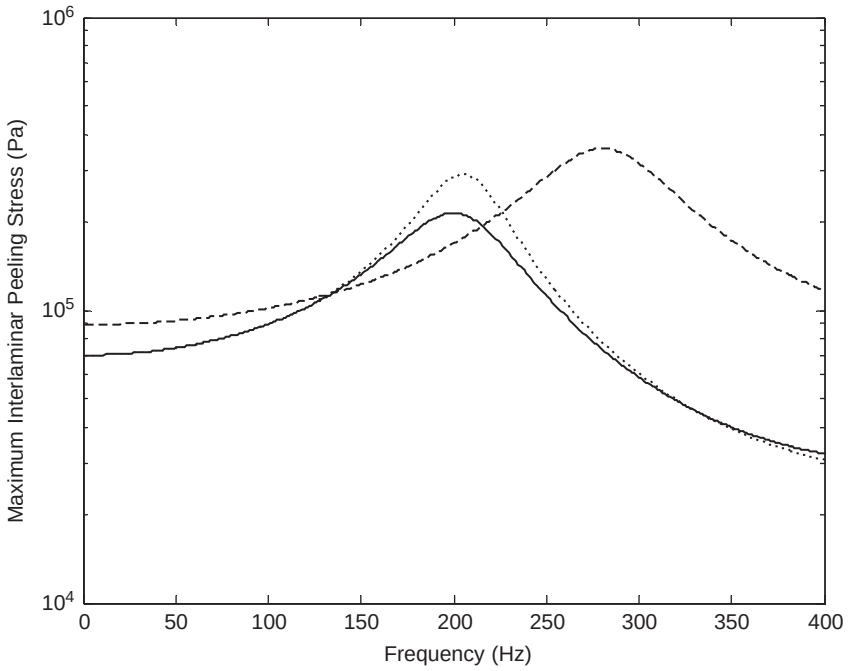

Fig. 18. Amplitude of peeling stress between VEM layer and beam for unit tip transverse load. Passive damping (· · · ·) max amplitude = 2.91×10^5 Pa; *D*-control (——) max amplitude = 2.15×10^5 Pa for $Kd = 191$; *P*-control (– – – –) resonant-amplitude = 3.57×10^5 Pa for $Kp = 1.5 \times 10^6$.

range of vibration reduction. Figs. 11 and 12 show the peak interlaminar peeling and shearing stresses, respectively (the tip displacement reduction of 3.14 dB corresponds to the maximum values in Figs. 7–9). It can be seen in these figures that the peak interlaminar peeling and shearing stresses are lower for derivative control as compared to proportional control. Also, the derivative control reduces the peak interlaminar peeling stress when compared to the passive damping case. The axial stress in PZT actuator for both of these cases is shown on Fig. 13. It can be seen in this figure that the axial stress in PZT is also lower for *D* control.

In summary, it is observed that in ACL treatments, derivative control can provide vibration reduction with lower control voltage, lower PZT axial stresses and lower interlaminar stresses than proportional control. Also, the interlaminar stresses for the derivative control scheme are even lower than those of the passive damping configuration due to lower levels of vibration. On the other hand, the proportional control increases the interlaminar stresses when compared to the passive damping case.

The study so far is conducted using 3MISD112 as the shear layer. To expand the investigation, another analysis is performed using a different VEM material for the shearing layer. The VEM selected is DYAD-606, which has a shear modulus of approximately 50 MPa and a loss factor of 1. This shear modulus is two orders of magnitude higher than that of the 3MISD112. Again, for this shearing layer, first the optimum thickness for passive damping (best fail safe) is calculated. Fig. 13 shows that the optimum thickness is 5.9 mm and the passive damping (1st mode critical damping ratio) for this thickness is 11.78%. It can be seem in Figs. 15–19 that the phenomenon

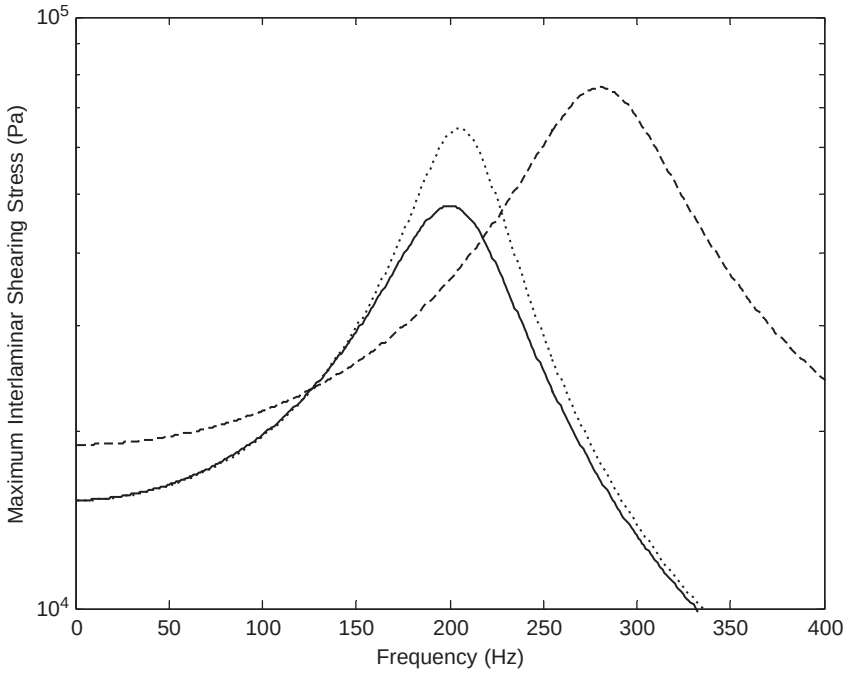

Fig. 19. Amplitude of shearing stress at both interfaces, PZT–VEM and VEM–beam, for unit tip load. Passive damping (· · · ·) resonant-amplitude = 6.49×10^4 Pa; *D*-control (——) resonant-amplitude = 4.8×10^4 Pa for $Kd = 191$; *P*-control (– – – –) resonant-amplitude = 7.6×10^4 Pa for $Kp = 1.5 \times 10^6$.

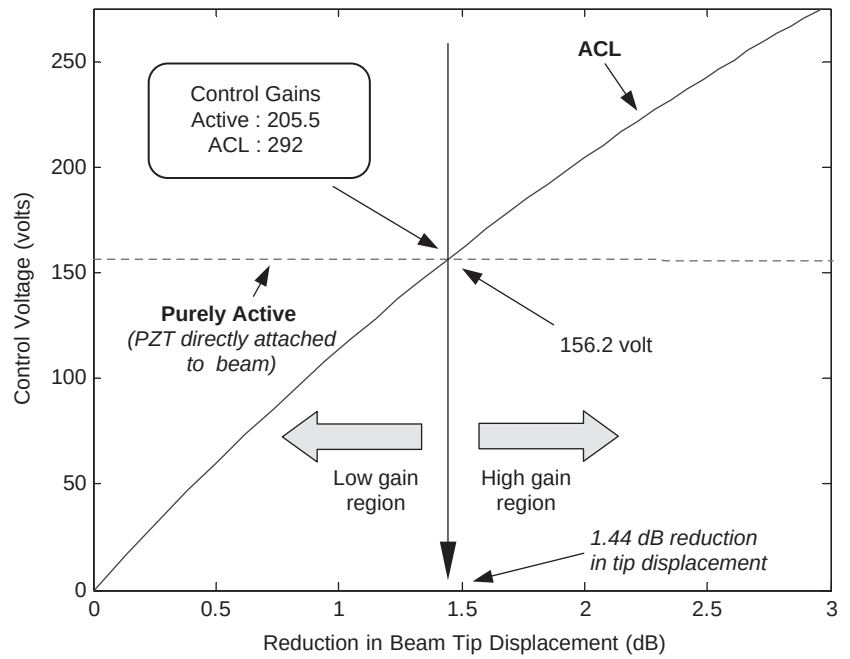

Fig. 20. Control voltage requirements for various vibration reduction values. Purely active control where PZT is directly attached to the beam (– – – –); ACL (——).

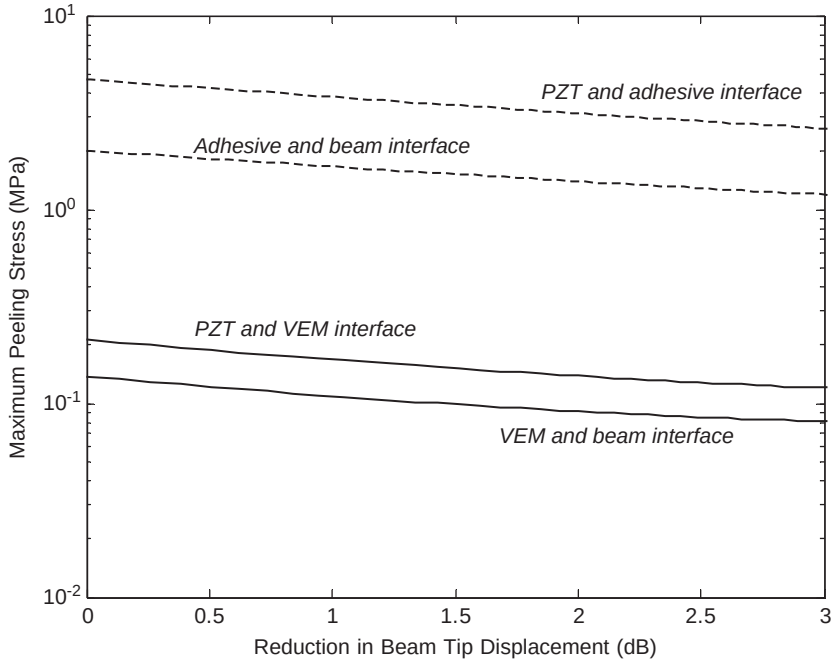

Fig. 21. Interlaminar peeling stress in purely active and ACL configurations. Purely active control where PZT is directly attached to the beam (– – – –); ACL (——).

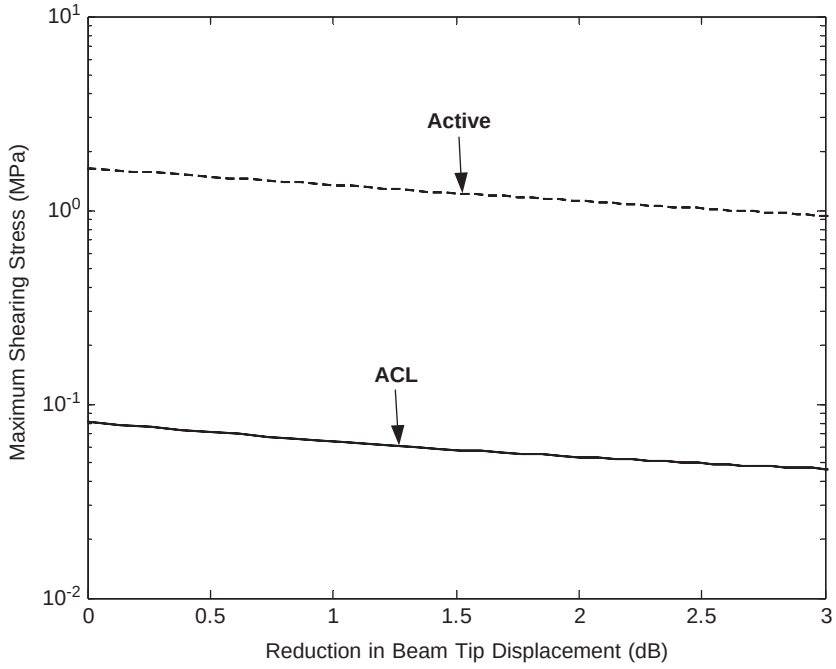

Fig. 22. Interlaminar shearing stress in purely active and ACL configurations. Purely active control where PZT is directly attached to the beam (– – – –); ACL (——).

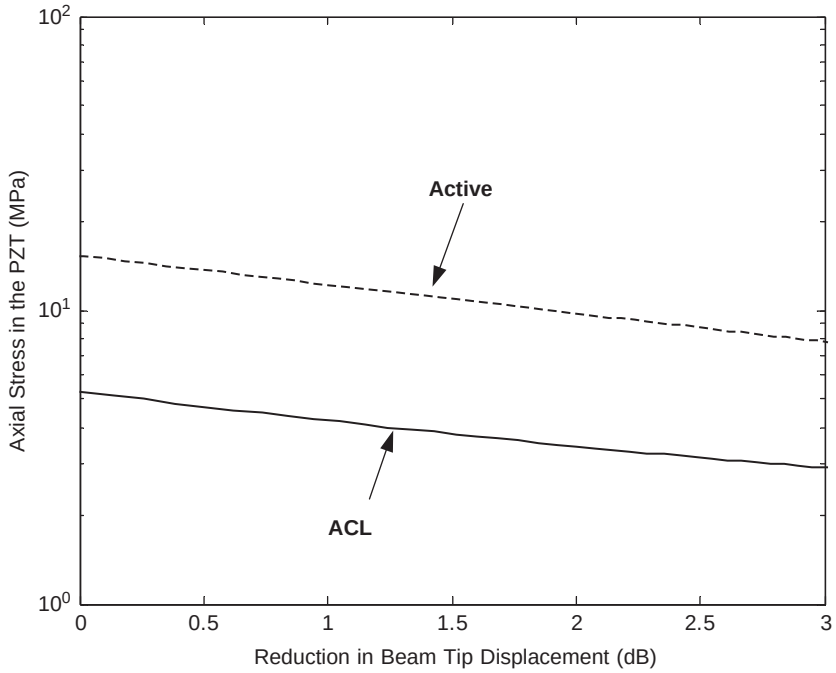

Fig. 23. PZT actuator axial stress in purely active and ACL configurations. Purely active control where PZT is directly attached to the beam (– – – –); ACL (——).

observed for the 3MISD112 material is also true for DYAD-606. That is, derivative control can provide the same level of attenuation of resonant response as proportional control but with lower voltage requirements and lower interlaminar stresses. Also, the maximum values of the interlaminar stresses for derivative control is lower than those of the passive damping case while proportional control increases the interlaminar stresses.

4.2. Comparison between ACL and purely active systems

The performance of ACL damping treatment has been compared with that of the purely active configuration (direct attachment of PZT on the host structure without VEM layer) by various researchers [8–12]. Liao and Wang [9,10] have shown that by a judicious choice of design parameters and control law, ACL could outperform the active configuration. Huang et al. [8] have shown that the ACL treatment could have better performance than a purely active configuration for low gain operations. Gandhi and Munsky [11,12] highlighted the importance of considering the piezoelectric layer voltage limits when evaluating the various configurations. All these comparison studies have focused mainly on the damping ability and/or control effort (voltage or power) requirements of the treatments.

In this investigation, the interlaminar stresses in the purely active configuration are compared with that in ACL (the 3MISD112 VEM is used in this study). The thickness of the adhesive in the purely active configuration is assumed to be same as that of optimum VEM thickness in the ACL,

which is 0.149 mm for 3MISD112. This is a reasonable thickness for epoxy layer in terms of fabrication considerations. To compare the ACL with the purely active configuration, the beam is excited with a unit tip force at first resonant frequency and the derivative control law (already proven to be a preferred choice) is used to reduce vibration. Fig. 20 plots the peak control voltage requirement as a function of the maximum beam tip displacement reduction. Note that as discussed earlier, for calculating the dB displacement reduction, the reference is chosen to be the maximum beam tip displacement of the passive damping system (constrained layer damping treatment with PZT coversheet and VEM layer but no active control), which is significantly lower than that of a system without any damping treatment. The reduction in maximum beam tip displacement increases with increasing control gain, that is, higher control gain provides larger vibration reduction. When the control gain is low (small vibration reduction), the required control effort (voltage) of the ACL is less than that of the purely active system. As the gain increases (for larger vibration reduction), the ACL would need a higher control voltage than the purely active configuration to achieve the same amount of reduction in beam tip displacement. Similar discussions on the effects of control gains on ACL vibration suppression performance and/or voltage requirements have also been presented in previous studies [8,10,12]. However, an important new observation here is that the active configuration has much (an order of magnitude) higher interlaminar stresses than the ACL treatment through out the range of vibration reduction being considered, as illustrated in Figs. 21 and 22. This indicates that while the performance (vibration reduction) and efficiency (control effort requirement) of the ACL could be better or worse than the purely active system depending on the limitations on control input (gains), its stress level is always much smaller. If the strength of the bond is the same for ACL and the purely active configuration, this would mean that the ACL treatment is much more durable. Fig. 23 shows the axial stress in the PZT actuator for the ACL and purely active configurations. It can be seen in this figure that the PZT axial stresses for the ACL configuration are considerably lower than the purely active case.

It can also be seen (Figs. 21–23) that with derivative control, the stresses decrease with increasing gain, due to the reduction in vibration amplitude. This is an important observation since it demonstrates that the actuator is more likely to delaminate when the controller is off. In other words, if the controller and the treatment are designed correctly, the reliability of the treatment could be improved due to feedback control for vibration suppression.

5. Summary

In this paper, the ACL treatment is analyzed for its interlaminar stress characteristics. It is demonstrated that for the system under consideration, derivative control has lower voltage requirements and interlaminar stresses as compared to the proportional control, given the same structural vibration level. The PZT actuator axial stresses are also lower for the derivative control scheme. This implies that the derivative control should be preferred over proportional control for ACL treatments. It is also shown that in comparison to a purely active configuration with similar vibration suppression performance, the interlaminar stress and PZT axial stress level in an ACL damping treatment could be an order of magnitude lower. This implies that if the strength of the bond is the same for ACL and the purely active configuration, the ACL treatment would be

significantly more durable. Another important observation in this investigation is that the interlaminar and axial stresses decrease with increasing derivative control gain (increasing control voltage). Hence, if derivative control is used, which is a preferred option due to lower stresses and control voltage, the treatment is less likely to delaminate when the controller is on. In other words, the active action will not only reduce vibration but also increase the system reliability.

Acknowledgements

This research was supported by the National Rotorcraft Technology Center with Dr. Yung Yu as technical monitor.

References

[1] J.M. Plump, J.E. Hubbard, Jr., Paper no. D4-1, Modeling of an active constrained layer damper, 12th International Congress on Acoustics, Toronto, Canada, 1986.
[2] G. Agnes, K. Napolitano, Active constrained layer viscoelastic damping, Proceedings of 34th AIAA/ ASME/ ASCE/ AHS/ ASC Structures, Structural Dynamics and Materials Conference, La Jolla, CA, 1993, pp. 3499–3506.
[3] A. Baz, J.-J. Ro, Performance characteristics of active constrained layer damping, in: C.D. Johnson (Ed.), Smart Structures and Materials 1994: Passive Damping, SPIE 2193, The International Society of Optical Engineering, Bellington, WA, 1994, pp. 98–114.
[4] I.Y. Shen, Stability and controllability of Euler–Bernoulli beams with intelligent constrained layer treatments, American Society of Mechanical Engineers, Journal of Vibration and Acoustics 118 (1996) 70–77.
[5] B. Azvine, G.R. Tomlinson, R.J. Wynne, Use of active constrained layer damping for controlling resonant vibration, Smart Materials and Structures 4 (1995) 1–6.
[6] M.J. Lam, W.R. Saunders, D.J. Inman, Modeling active constrained layer damping using Golla-Hughes-McTavish approach, in: C.D. Johnson (Ed.), Smart Structures and Materials 1995: Passive Damping, SPIE 2445, The International Society of Optical Engineering, Bellington, WA, 1995, pp. 86–97.
[7] G.A. Lesieutre, U. Lee, A finite element for beams having segmented active constrained layers with frequency-dependent viscoelastic, Smart Materials and Structures 5 (1996) 615–627.
[8] S.C. Huang, D.J. Inman, E.M. Austin, Some design considerations for active and passive constrained layer damping treatments, Smart Materials and Structures 5 (1996) 301–313.
[9] W.H. Liao, K.W. Wang, On the active-passive hybrid control actions of active constrained layers, American Society of Mechanical Engineers, Journal of Vibration and Acoustics 119 (1997) 563–572.
[10] W.H. Liao, K.W. Wang, On the analysis of viscoelastic materials for active constrained layer damping treatments, Journal of Sound and Vibration 207 (1997) 319–334.
[11] F. Gandhi, B. Munsky, Comparison of damping augmentation mechanisms with position and velocity feedback in active constrained layer treatments, Journal of Intelligent Material Systems and Structures 13 (5) (2002) 259–326.
[12] F. Gandhi, B. Munsky, Effectiveness of active constrained layer damping treatments in attenuating resonant oscillations, Journal of Vibration and Control 8 (2002) 747–775.
[13] W. Seemann, K.D. Wolf, A. Straub, P. Hagedon, F.K. Chang, Bonding stresses between piezoelectric actuators and elastic beams, in: M.E. Rengelbrugge (Ed.), Smart Structures and Materials 1997: Smart Structures and Integrated Systems, SPIE 3041, The International Society of Optical Engineering, Bellington, WA, 1997, pp. 665–675.
[14] A. Badre-Alam, K.W. Wang, F. Gandhi, Optimization of enhanced active constrained layer (EACL) treatment on helicopter flexbeams for aeromechanical stability augmentation, Smart Materials and Structures 8 (1999) 182–196.

[15] U. Lee, G.A. Lesieutre, Reliability of the piezoelectric layer application to vibration and noise control, Journal of Vibration and Acoustics 121 (1999) 137–139.
[16] A. Badre-Alam, F. Gandhi, K.W. Wang, Improved constrained layer damping treatment for high damping and low interlaminar stresses, in: T. Tupper Hyde (Ed.), Smart Structures and Materials 2000: Damping and Isolation, SPIE 3989, The International Society of Optical Engineering, Bellington, WA, 2000, pp. 2–13.
[17] B. Mirman, Interlaminar stresses in layered beams, American Society of Mechanical Engineers, Journal of Electronic Packaging 114 (1992) 384–388.
[18] B. Mirman, Microelectronics and the Built-Up-Bar theory, American Society of Mechanical Energy, Journal of Electronic Packaging 114 (1992) 389–396.
[19] E. Suhir, Stresses in Bi-Metal thermostats, American Society of Mechanical Energy, Journal of Applied Mechanics 53 (1986) 657–660.
[20] E. Suhir, Interfacial stresses in Bi-Metal thermostats, American Society of Mechanical Energy, Journal of Applied Mechanics 56 (1989) 595–600.
[21] Y.-H. Pao, E. Eisele, Interfacial shear and peeling stresses in multilayered think stacks subjected to uniform thermal loading, American Society of Mechanical Engineers, Journal of Electronic Packaging 113 (1991) 164–172.
[22] L. Lee, B. Mirman, Bending stiffness of a multilayered structure, Proceedings of International Electronics Packaging Conference, Marlborough, MA, 1990, pp. 150–164.
[23] E. Ponslet, R.T. Haftka, N.H. Cudney, Model reduction and eigenvalue sensitivity for controlled structures, Computers and Structures 51 (1994) 373–379.
[24] M.I. Friswell, D.J. Inman, Finite element models with viscoelastic damping, Proceedings of the 17th International Modal Analysis Conference, Kissimmee, FL, 1999, pp. 181–187.
[25] A.-S. Plouin, E. Balmes, Pseudo-modal representations of large models with viscoelastic behavior, Proceedings of the International Modal Analysis Conference, Santa Barbarca, CA, 1998, pp. 1440–1446.
[26] A. Badre-Alam, Aeromechanical stability augmentation of helicopters using enhanced active constrained layer damping treatment, Ph.D. Dissertation, The Pennsylvania State University, 2000.